IV

Publication IV

T. Kurki-Suonio, V. Hynönen, T. Ahlgren, K. Nordlund, K. Sugiyama, R. Dux, and the ASDEX Upgrade Team (2007). Fusion tritons and plasma-facing components in a fusion reactor. *Europhysics Letters*[†] **78**(6) 65 002 (6 pp).

[†] http://www.epljournal.org/

A Letters Journal Exploring the Frontiers of Physics

June 2007

EPL, **78** (2007) 65002
doi: 10.1209/0295-5075/78/65002

www.epljournal.org

Fusion tritons and plasma-facing components in a fusion reactor

T. Kurki-Suonio[1(a)], V. Hynönen[1], T. Ahlgren[2], K. Nordlund[2], K. Sugiyama[3], R. Dux[4] and the ASDEX Upgrade Team[4]

[1] *Advanced Energy Systems, Helsinki University of Technology, Association Euratom-TEKES - P.O. Box 4100, FI-02015 TKK, Finland*
[2] *Accelerator Laboratory - P.O. Box 43, University of Helsinki, FI-00014 Helsinki, Finland*
[3] *Interdisciplinary Graduate School of Engineering Sciences, Kyushu University - Hakozaki 6-10-1, Higashi-ku, Fukuoka 812-8581, Japan*
[4] *Max-Planck-Institut für Plasmaphysik, Euratom Association - D-85740 Garching, Germany*

received 24 January 2007; accepted in final form 7 May 2007
published online 1 June 2007

PACS 52.40.Hf – Plasma-material interactions; boundary layer effects
PACS 52.55.Fa – Tokamaks, spherical tokamaks
PACS 52.55.Pi – Fusion products effects (*e.g.*, alpha-particles, etc.), fast particle effects

Abstract – We would like to discuss the role that 1 MeV tritons produced in deuterium–deuterium fusion reactions might play in a long-pulse or steady-state fusion reactor. Albeit a small minority in quantity compared to the fuel tritium, the fusion tritons have significantly longer penetration length in materials and can have detrimental consequences for the integrity of the components. Because deeply deposited atoms are not easily removed from the plasma-facing components, the fusion tritium inventory in a steady-state device is expected to be limited only by decay. Furthermore, unlike fuel tritium, it is not evenly distributed on the plasma-facing components. We conclude that, of the materials considered here, tungsten appears better than carbon or beryllium in this respect. Nonetheless, 1 MeV tritons from deuterium fusion should not be neglected when making material choices for ITER and, especially, for future fusion reactors. In particular, studies on the bulk effects of deeply penetrated tritium in tungsten are urgently needed if metal-wall reactors are considered for the future. This is an interdisciplinary problem needing the attention of material scientists and plasma physicists.

Introduction. – Fusion energy holds a great promise. It is inherently safe, produces no long-term radio-active waste or gases contributing to the green house effect, and the fuel exists in abundance. One of the main concerns in a future fusion reactor will be the interface between the hot plasma and the cold vessel wall. It affects the choice of the plasma parameters, the engineering design of the machine and the material selection of the plasma-facing surfaces.

In future fusion reactors the long-term tritium retention will be a critical issue. In a fusion reactor, the fuel consists of deuterium and tritium, and in the case of a loss-of-vacuum accident, the radioactive tritium (half-life 12.3 years) released into the atmosphere must not pose a safety hazard to the population. For this reason all nuclear facilities are licensed with a site inventory limit for tritium and other radioactive substances. In ITER, which will be the first device to demonstrate a burning plasma, the in-vessel tritium inventory limit will be 350 g.

The amount of fuel instantaneously in the plasma volume will, of course, never exceed the site limit. However, since the anticipated burn-up rate of tritium is quite small, about 1% for ITER [1], some of the fuel tritium will diffuse out of the bulk plasma and adhere to the vessel walls, thus accumulating over the operation. The primary retention mechanism of tritium is co-deposition with eroded first-wall material. This is particularly effective in the case of carbon, because tritium readily forms hydrocarbons that, in turn, form films on the material surfaces. At high temperatures, these films are easily decomposed when exposed to air [2] and, thus, pose a potential safety hazard in the case of a vacuum leak. Furthermore, the measured tritium build-up rates at JET and TFTR tokamaks, both of which were operating with carbon walls at the time, are too high for ITER [3]. For these reasons there is today a growing interest

(a) E-mail: taina.kurki-suonio@tkk.fi

in carbon-free fusion machines: ASDEX Upgrade in Garching, Germany, has replaced, step-by-step, all carbon fibre composite structures by tungsten-coated ones [4,5], while on Alcator C-Mod at MIT, Cambridge, USA, molybdenum has been intensely investigated as a first-wall material candidate [6,7]. The present ITER design is based on using three different materials for the plasma-facing components: tungsten, beryllium and carbon.

The tritium inventory from the fuel tritium is typically found on top of the material surfaces, where it is deposited as amorphous hydrogen-rich carbon layers. This is because the fuel tritons are thermal, *i.e.*, have low energy ($E \lesssim 100\,\mathrm{eV}$) and, thus, a penetration depth of at most a few nanometers. The advantage of surface deposition is that various techniques of removing the contaminated films from the surfaces exist [2], at least in principle. However, tritium is also formed in deuterium–deuterium (D–D) reactions. The quantity of tritium formed inside the plasma will be insignificant compared to the amount of fuel tritium: the D–D fusion reaction rate is about 1/200 of the deuterium–tritium reaction rate [8]. But due to its very high energy, contribution of the fusion-born tritium to the long-term tritium inventory and material damages can still be significant. Until now, with few exceptions [9,10], most of the studies on tritium retention have concentrated on thermal tritium that can penetrate the material only by diffusion. The implantation of tritium has been considered only for energies up to keV range [11].

In this paper we briefly discuss the relevance of the fusion-born tritium for ITER and for a fusion reactor that is supposed to operate on steady-state basis. Of the materials, the emphasis is on tungsten because, although ITER will use beryllium as the first-wall material, future power reactors are envisaged to operate with heavy-metal walls. The discussion is supplemented by both experimental and numerical results from the ASDEX Upgrade tokamak.

High-energy tritons from D–D reactions. – The fusion tritons are produced in one of the two D–D reaction branches,

$$\mathrm{D} + \mathrm{D} \rightarrow {}^3\mathrm{He}(0.82\,\mathrm{MeV}) + \mathrm{n}(2.45\,\mathrm{MeV})$$

$$\mathrm{D} + \mathrm{D} \rightarrow \mathrm{T}(1.01\,\mathrm{MeV}) + \mathrm{p}(3.02\,\mathrm{MeV}).$$

Since the reaction rates for the two branches are practically equal in the relevant temperature range (up to a few tens of keVs) [8], the triton source rate can be experimentally inferred from the measured neutron rate. Due to their wide drift orbits, the 1 MeV tritons have a much higher probability of escaping the plasma at high energy and, because of their high energy, they penetrate a lot deeper, up to ten micrometers, in the material structures of the vacuum vessel.

The loss rate at high energies is enhanced by the so-called ripple diffusion, always present in a tokamak with a finite number of toroidal field coils. The loss of axisymmetry makes the trapped banana orbits to become

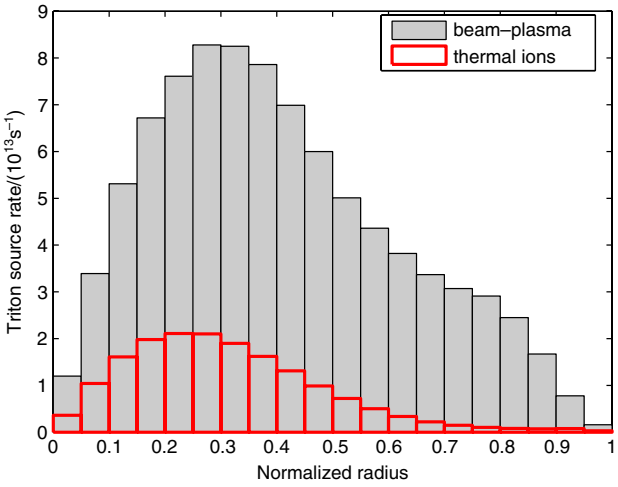

Fig. 1: (Colour on-line) The triton source rate for beam–plasma (grey bars) and thermal (red/grey thick-lined bars) D–D reactions calculated for ASDEX Upgrade shot # 17219. Reprinted with permission from fig. 21, ref. [12]. © Copyright 2007 by IOP Publishing Limited.

stochastic and can lead the tritons out of the plasma before they have had enough time to slow down significantly. This mechanism leads to increased triton flux, particularly on the low-field side of the vessel. The effect of the toroidal ripple on fast-particle losses in ASDEX Upgrade has been evaluated using the orbit-following Monte Carlo code ASCOT [12], where it was found to increase the wall load by 50%. The effect of ripple on high-energy tritons has also been observed experimentally [10].

An order of magnitude estimate for the amount of D–D tritium produced in one 400 s ITER pulse can be obtained separately for the thermal deuterium ions and for the reactions with neutral beam ions. In contemporary tokamaks, fusion tritium is formed mostly in beam–plasma reactions. Figure 1 shows the triton source rate for beam–plasma reactions and thermal ions calculated for ASDEX Upgrade pulse #17219, and the dominance of beam–plasma reactions is obvious. In the ITER inductive operating scenario [13], the average electron density is $\langle n_\mathrm{e}\rangle = 10.1 \times 10^{19}\,\mathrm{m}^{-3}$. Neglecting the impurities this is equal to the deuteron density, $\langle n_\mathrm{D}\rangle = \langle n_\mathrm{e}\rangle$. The D–D reactivity for average ion temperature $\langle T_\mathrm{i}\rangle = 8\,\mathrm{keV}$ in the inductive scenario is $\langle \sigma v\rangle = 3.4 \times 10^{-25}\,\mathrm{m}^3/\mathrm{s}$ [8]. The plasma volume is $V = 831\,\mathrm{m}^3$, so that a rough estimate for the amount of tritium produced by thermal ions is

$$m_\mathrm{T,th} = \frac{1}{2}\langle n_\mathrm{D}\rangle^2 \langle \sigma v\rangle\, V \times 400\,\mathrm{s} \times 3\,\mathrm{amu}$$

$$\approx 2.8\,\mathrm{mg/pulse}.$$

The two heating and current drive injectors in ITER deliver deuterium beams with a total power of 33 MW and nominal energy of 1 MeV, which equals to 2.06×10^{20} particles per second. A more detailed calculation would require information about the steady-state distributions

of beam particles, but since the slowing-down time of 1 MeV is of the order of seconds, a reasonable estimate can be acquired by assuming 2×10^{20} 1 MeV deuterons distributed homogeneously in the plasma. The velocity and the fusion cross-sections of 1 MeV deuterons are $v = 9.8 \times 10^6$ m/s and $\sigma = 8.7 \times 10^{-30}\,\mathrm{m}^2$ [8]. With these assumptions we get

$$m_{\mathrm{T,beam}} = \langle n_{\mathrm{D}} \rangle \frac{2 \times 10^{20}}{V} \sigma v \times V \times 400\,\mathrm{s} \times 3\,\mathrm{amu} \approx 3.5\,\mathrm{mg/pulse}$$

for the amount of tritium produced in beam–plasma reactions. Even though only a part of the tritium produced in D–D reactions comes out of the plasma with high energy, it still means a few milligrams per pulse. On JT-60 about one third of the fusion tritium have been found to reach the walls in OFMC simulations [9], and similar numbers are obtained for ASDEX Upgrade in Ascot simulations (see the following section and ref. [12]).

In order to carry on the order-of-magnitude estimate to the tritium inventory in ITER and in a steady-state device, we will assume that the only mechanism limiting the amount of tritium in the wall is its radioactive decay, *i.e.*, we neglect any other saturation effects. Assuming a constant source rate S, the time dependence of tritium inventory in this case can be solved from

$$\frac{\mathrm{d}N}{\mathrm{d}t} = S - \lambda N,$$

giving $N(t) = S/\lambda[1 - \exp(-\lambda t)]$. In the limit $t \to \infty$ the steady-state inventory will be $N_\infty = S/\lambda$. Assuming 1 mg of tritium to be implanted in one 400 s ITER pulse, and 12 000 pulses distributed uniformly over 10 years (see ref. [11]), this gives $N_\infty = 20$ g. In 10 years the inventory will be $N(t = 10\,\mathrm{a}) = 9$ g. However, assuming the same source rate of $S = 1\,\mathrm{mg}/400\,\mathrm{s}$ in a steady-state device leads to $N_\infty = 1.4$ kg. In reality the source rate is likely to be larger, and already in ITER additional energetic tritons in the MeV range are produced by ion cyclotron resonance heating.

Using the SRIM2003 code (the Stopping and Range of Ions on Matter) [14] with the default parameters for density and normal angle of incidence, we obtained the mean ranges for 1 MeV and 100 eV tritons in carbon (at graphite density of $2.25\,\mathrm{g/cm}^3$), tungsten and beryllium as shown in table 1. Although the nuclear and electronic stopping powers in SRIM are known to have systematic uncertainties of the order of 10% [15,16], such possible uncertainties are not significant for the further discussion in the current paper.

In tungsten, it has been experimentally observed that at room temperature the deuterium retention in tungsten increases with implantation energy. At deuterium implantation energy of 5 keV, at low fluences ($\lesssim 10^{21}\,\mathrm{m}^{-2}$) only about 7% of deuterium is retained in polycrystalline tungsten. This retained amount then rapidly increases with implantation energy up to 22% and 55% for implantation energies 15 keV and 30 keV, respectively [17]. Thus, at MeV implantation energies virtually all implanted tritium is retained at low fluences. There are two reasons for this: firstly, implantation with higher energy creates more implantation-induced damage to which tritium is trapped, and secondly, the deeper projected range increases the probability of tritium to be trapped in inner walls of intrinsic microscopic cavities localized at grain boundaries [18].

Table 1: The mean range of tritons in carbon, tungsten and beryllium at energies 100 eV and 1 MeV.

Implant. energy	100 eV	1 MeV
tungsten	(2.8 ± 1.5) nm	$(4.3 \pm 0.1)\,\mu$m
carbon	(2.8 ± 1.6) nm	$(7.7 \pm 0.1)\,\mu$m
beryllium	(3.3 ± 1.6) nm	$(10.2 \pm 0.1)\,\mu$m

Table 2: The backscattered fraction of implanted atoms at energies 100 eV and 1 MeV.

Implant. energy	100 eV	1 MeV
tungsten	(47.1 ± 0.2)%	(0.11 ± 0.01)%
carbon	(9.9 ± 0.1)%	(0.000 ± 0.001)%
beryllium	(6.2 ± 0.1)%	(0.000 ± 0.001)%

Another effect that increases the retention of tritium in materials with increasing implantation energy is the rapid decrease of backscattering probability with implantation energy. Table 2 shows how about 47% of 100 eV tritium atoms hitting tungsten are backscattered into the plasma, while at 1 MeV the backscattering probability is almost zero. The combined effect of reduced backscattering probability and increased retention of tritium at implantation energies of 1 MeV compared to 100 eV further enhances the importance of D–D reaction considering the total tritium inventory in fusion reactors.

Estimating the retention of deuterium in tungsten becomes more complicated at high deuterium fluences ($> 10^{22}\,\mathrm{m}^{-2}$). According to Haasz *et al.* [19], at implantation energy of 0.5 keV, the saturation retention of deuterium is about $5 \times 10^{20}\,\mathrm{m}^{-2}$ for implantation fluences between $10^{21}\,\mathrm{m}^{-2}$ and $10^{24}\,\mathrm{m}^{-2}$. In another study with larger implantation energy of 6 keV and fluence of $10^{23}\,\mathrm{m}^{-2}$, the deuterium saturation concentration was about $5 \times 10^{27}\,\mathrm{m}^{-3}$. This corresponds to about 10 atomic percent of deuterium in tungsten [20]. The projected range of 6 keV deuterium is about 50 nm, but the deuterium concentration was found to display a slowly decreasing tail extending beyond 2 μm. Thus, for the 1 MeV tritons, assuming a similar saturation concentration extending many times the projected range of 4.3 μm the retention could be more than $5 \times 10^{22}\,\mathrm{m}^{-2}$. With a $1000\,\mathrm{m}^2$ tungsten wall, the saturation tritium amount in the implanted zone could reach 250 g. The rest of the tritium not retained in the implantation zone would have been released back to the plasma or would have diffused deeper into the tungsten wall.

At high fluences there will be another effect on the retention, namely blistering. When the fluence and flux are high enough so that hydrogen diffusion and defect recovery are slow, hydrogen starts to form bubbles in the material. The blister size increases with implantation energy [21]. When the blisters rupture, hydrogen retained in the wall is released.

We also consider whether the beta decay of tritium affects the bubble and/or bulk material properties. The kinetic energy of the beta particle (electron) produced in the decay is 18.6 keV, which leads, due to the conservation of energy and momentum, to a recoil energy of about 3 eV for the resulting ^{3}He atom. This energy is well below the threshold displacement energy of both carbon and common metals [22]. Also the 18.6 keV electron could, in principle, cause damage in materials when it collides with sample atoms. However, the maximum recoil energy that an electron of this energy can transfer in a head-on collision to a Be- or C-atom is about 4 eV, and for a W-atom only 0.2 eV, which is also well below the threshold displacement energies in these materials [22]. Hence we conclude that the beta decay of tritium does not alter material properties significantly.

On the other hand, once the tritium has converted into a ^{3}He (if the tritium still remains in the sample), it will chemically behave like a helium rather than a hydrogen atom. He-atoms are known to produce damage in materials quite differently compared to hydrogen, *e.g.* helium forms bubbles very differently in tungsten than in hydrogen [18]. Thus for any tritium retained in the samples for time scales comparable to its half-life, not only the damage effects due tritium but also due to helium need to be considered.

Due to the exceptionally fast diffusion of hydrogen, only trapped hydrogen is present in tungsten at room temperature [23]. The release of hydrogen from polycrystalline tungsten starts at about 445 K [24], and practically all implanted hydrogen is removed from tungsten at about 900 K [17]. The high-energy tritium can thus be removed from tungsten at reasonable temperatures. In carbon, the removal of deeply penetrated tritium is considerably more difficult. The slower diffusion together with the quite strong binding of hydrogen atoms to the amorphous carbon matrix results in that temperatures between 1200 K and 1300 K, depending on carbon density, are needed to remove all hydrogen in a few hours [25,26].

D–D **tritium surface distribution in ASDEX Upgrade.** – To illustrate how fusion tritons are distributed in a fusion device, we now simulate the tritium wall distribution in ASDEX Upgrade using the ASCOT code. In the past, quantitative measurements of the tritium inventory were carried out for selected wall tiles in ASDEX Upgrade [27]. These measurements extended up to 25 μm, and gave maximum concentrations of the order of several 10^{-8} T/C (tritium atoms per carbon atom) in the private flux region. For comparison, the measured deuterium

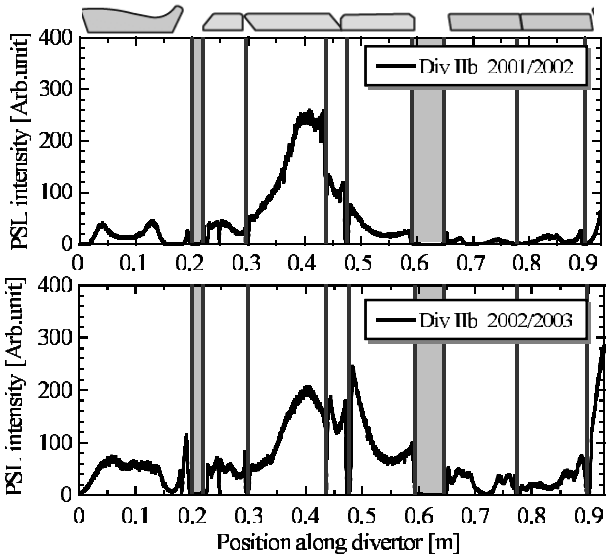

Fig. 2: The measured Photo-Stimulate Luminescence (PSL) intensity on the divertor from ASDEX Upgrade campaigns 2001/2002 and 2002/2003. Reprinted with permission from fig. 24, ref. [12]. © Copyright 2007 by IOP Publishing Limited.

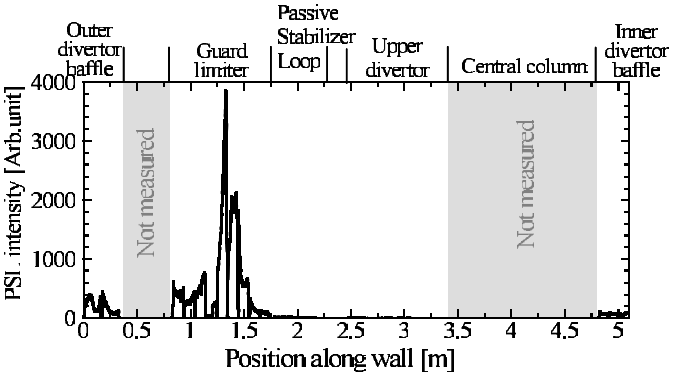

Fig. 3: The measured Photo-Stimulate Luminescence (PSL) intensity on the wall from ASDEX Upgrade campaign 2002/2003. Reprinted with permission from fig. 25, ref. [12]. © Copyright 2007 by IOP Publishing Limited.

concentrations at the depth of 20 μm were found to be several 10^{-4} D/C [28]. Qualitatively, the distribution of tritium surface deposition has been studied by Photo-Stimulate Luminescence (PSL) measurements carried out at JT-60U [29] and at ASDEX Upgrade [30]. Recent measurement results on ASDEX Upgrade are shown in figs. 2 (divertor region) and 3 (first wall). The highest tritium levels are found at the top of the divertor dome and at the guard limiter. The PSL intensity on the wall, and especially in the vicinity of the guard limiter, is an order of magnitude higher than on the divertor, but the intensities on the wall and on the divertor are not directly comparable because the wall is not axisymmetric.

As mentioned, the fuel tritium is predominantly co-deposited with eroded first-wall material, but in D–D discharge machines the tritium distribution on the

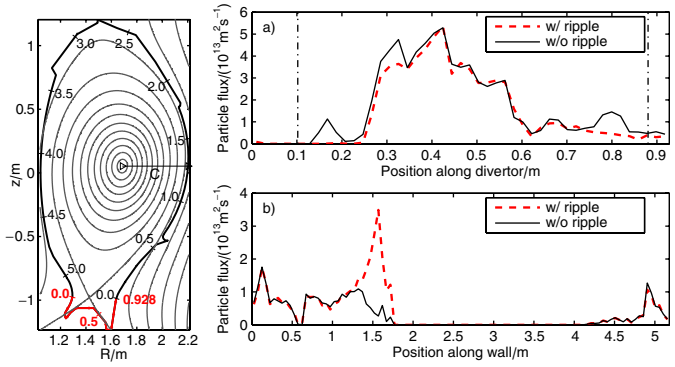

Fig. 4: (Colour on-line) The triton flux a) onto the divertor and b) onto the wall structures in the axisymmetrical case (solid line) and in the case with finite toroidal ripple (red/grey thick dashed line). The strike-points are marked with vertical dash-dotted lines in a), and the coordinates are illustrated on the left. Reprinted with permission from figs. 1 and 22, ref. [12]. © Copyright 2007 by IOP Publishing Limited.

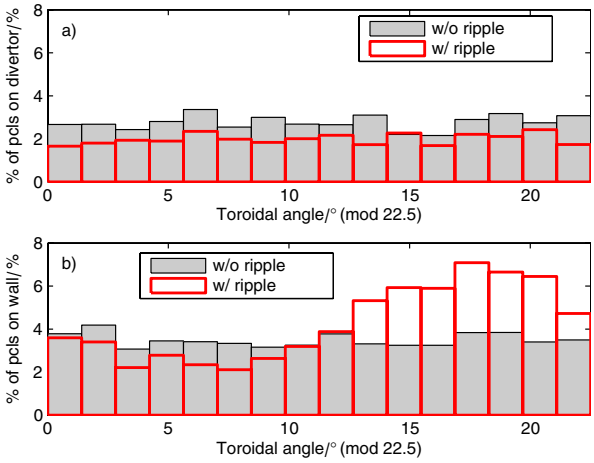

Fig. 5: (Colour on-line) The toroidal distribution of the triton flux a) onto the divertor and b) onto the wall structures in the axisymmetrical case (grey bars) and in the case with finite toroidal ripple (red/grey thick-lined bars). Reprinted with permission from fig. 23, ref. [12]. © Copyright 2007 by IOP Publishing Limited.

plasma-facing components has been found to be similar to the distribution of high-energy triton implantation [29,30]. To confirm these findings, the D–D-triton flux onto the material surfaces was simulated. The measured distribution and the simulated flux can be compared qualitatively, because the former is the time integral of the latter, neglecting the decay.

The measured tritium in the surface materials has been accumulating over time and during various kinds of discharges, of which the H-mode is the most typical one. The magnetic and plasma backgrounds for the simulations were obtained from the improved H-mode discharge #17219 at $t = 2.5\,\mathrm{s}$. The initial energy of tritons is 1.008 MeV, and in the simulations the pitch was assumed to be uniformly distributed. This is a reasonable assumption, since the initial energy of tritons is high even compared to the nominal injection energy of the neutral beams. Figure 1 shows the calculated source rate of tritons as a function of normalized radius ρ. Due to the fast parallel motion of beam ions, the tritons were assumed to be born uniformly along a flux surface.

An ensemble of 12 500 test particles was used and the particles were given weights according to the local volume element along a single flux surface and according to the triton source rate in the ρ-direction. The particles were simulated with and without ripple until they were thermalized, and the hits on the material surfaces were recorded.

Using the ASDEX Upgrade ripple values, the fraction of particles hitting the divertor was 11%, while the wall load was 24% of the total number of particles. Figure 4 shows the triton flux onto the divertor and onto the wall. For an axisymmetric case (no ripple) the divertor flux is practically the same (about 13%), but on the wall the flux onto the guard limiter ($s_\mathrm{w} \approx 1.5\,\mathrm{m}$) is significantly higher with ripple (total load with axisymmetic magnetic field was only about 16%). Figure 5 shows the toroidal distribution of the triton flux on the divertor and on the wall. The divertor load is always uniform in the toroidal direction, whereas the load to the first wall varies by a factor of three.

The simulated flux and the measured PSL intensity are in qualitative agreement. According to fig. 4, the region of largest triton flux is the private flux region. Furthermore, the energy of tritons ending up in the private flux region is found to be very close to the initial 1 MeV. The average energy of the limiter particles is fortunately lower (600 keV) because the stochastic diffusion is slow compared to the almost instantaneous losses to the private flux region, thus giving the particles more time to slow down. It should be noted that, even in the simulations where the magnetic field was non-axisymmetric due to the ripple, the wall structures were still taken toroidally symmetric. This means that the ripple-induced enhancement in the triton flux to the guard limiter is in reality necessarily much higher than implied in fig. 4.

Conclusions. – We conclude that the fusion-born tritium deserves a careful consideration in fusion reactors due to its high birth energy and deep penetration. In principle it can contribute to both material damage and total tritium inventory in the machine.

As for the tritium inventory, the D–D tritium constitutes only a small quantity compared to the fuel tritium, but its deposition into materials is very different: while fuel tritium is predominantly deposited on the wall surface layers and is thus, at least in principle, easily removable, the D–D tritium penetrates deep into the material. Of the wall materials considered for ITER and DEMO, *i.e.*, beryllium, carbon and tungsten, the last one appears best-behaved in this respected because of the exceptionally fast diffusion of hydrogen isotopes in

tungsten. Thus even deeply deposited tritium could be removed by heating the walls.

It should, however, be born in mind that the dominant mechanism bringing the D–D tritium out of the plasma is stochastic ripple diffusion, and the same mechanism also spits out 3.5 MeV fusion alphas. Helium is known to create bubbles in bulk material and tritium can get trapped into these bubbles. This tritium is harder to remove and can thus contribute to the long-term tritium inventory even with machine baking.

Studies on the bulk effects of deeply penetrated tritium in first-wall relevant materials are urgently needed. This is an interdisciplinary problem needing the attention of material scientists, plasma physicists and fusion experiments. In 2007, ASDEX Upgrade will be operating as a carbon-free fusion device with tungsten wall and divertor, thus producing unprecedented data for the wall deposition of hydrogen isotopes in the absence of carbon. In 2008, after regaining all its power sources, ASDEX Upgrade would also have ITER-relevant heating capabilities normalized to its size and, thus, could provide a suitable test bed for material studies of D–D-tritium effects.

* * *

This work, supported by the European Communities, under the contract of Association between Association Euratom/Tekes, was carried out within the framework of the European Fusion Development Agreement. The views and opinions expressed herein do not necessarily reflect those of the European Commission. The ASCOT computations presented in this document have been made with CSC's computing environment. CSC is the Finnish IT center for science and is owned by the Ministry of Education.

REFERENCES

[1] Gouge M. J., *Fusion Technol.*, **35** (1998) 435.
[2] Federici G., Skinner C. H., Brooks J. N., Coad J. P., Grisolia C., Haasz A. A., Hassanein A., Philipps V., Pitcher C. S., Roth J., Wampler W. R. and Whyte D. G., *Nucl. Fusion*, **41** (2001) 1967.
[3] Andrew P., Brennan D., Coad J. P., Ehrenberg J., Gadeberg M., Gibson A., Groth M., How J., Jarvis O. N., Jensen H., Lässer R., Marcus F., Monk R., Morgan P., Orchard J., Peacock A., Pearce R., Pick M., Rossi A., Schunke B., Stamp M., von Hellermann M., Hillis D. L. and Hogan J., *J. Nucl. Mater.*, **266-269** (1999) 153.
[4] Neu R., Asmussen K., Deschka S., Thoma A., Bessenrodt-Weberpals M., Dux R., Engelhardt W., Fuchs J. C., Gaffert J., García-Rosales C., Herrmann A., Krieger K., Mast F., Roth J., Rohde V., Weinlich M., Wenzel U., ASDEX Upgrade Team and ASDEX NI-Team, *J. Nucl. Mater.*, **241-243** (1997) 678.
[5] Neu R., Dux R., Geier A., Greuner H., Krieger K., Maier H., Pugno R., Rohde V., Yoon S. W. and ASDEX Upgrade Team, *J. Nucl. Mater.*, **313-316** (2003) 116.
[6] Pappas D. A., Lipschultz B., LaBombard B., May M. J. and Pitcher C. S., *J. Nucl. Mater.*, **266-269** (1999) 635.
[7] Lipschultz B., Pappas D. A., LaBombard B., Rice J. E., Smith D. and Wukitch S., *J. Nucl. Mater.*, **290-293** (2001) 286.
[8] Bosch H.-S. and Hale G. M., *Nucl. Fusion*, **32** (1992) 611.
[9] Tanabe T., Bekris N., Coad P., Skinner C. H., Glugla M. and Miya N., *J. Nucl. Mater.*, **313-316** (2003) 478.
[10] Tobita K., Nishio S., Konishi S., Sato M., Tanabe T., Masaki K. and Miya N., *Fusion Eng. Design*, **65** (2003) 561.
[11] Federici G., Brooks J. N., Iseli M. and Wu C. H., *Phys. Scr.*, **T91** (2001) 76.
[12] Hynönen V., Kurki-Suonio T., Suttrop W., Dux R., Sugiyama K. and the ASDEX Upgrade Team, *Plasma Phys. Control. Fusion*, **49** (2007) 151.
[13] ITER technical basis, ITER EDA Documentation Series (IAEA, Vienna, Austria) 2001 `http://www.iter.org/reports.htm`.
[14] Ziegler J. F., SRIM-2003 software package `http://www.srim.org`.
[15] Haussalo P., Nordlund K. and Keinonen J., *Nucl. Instrum. Methods Phys. Res., Sect. B*, **111** (1995) 1.
[16] Nordlund K., Runeberg M. and Sundholm D., *Nucl. Instrum. Methods Phys. Res., Sect. B*, **132** (1997) 45.
[17] Heinola K., Ahlgren T., Vainonen-Ahlgren E., Likonen J. and Keinonen J., *Phys. Scr.*, **T128** (2007) 91.
[18] Henriksson K. O. E., Nordlund K., Krasheninnikov A. and Keinonen J., *Appl. Phys. Lett.*, **87** (2005) 163113.
[19] Haasz A. A., Poon M., Macaulay-Newcombe R. G. and Davis J. W., *J. Nucl. Mater.*, **290-293** (2001) 85.
[20] Alimov V. K., Ertl K. and Roth J., *J. Nucl. Mater.*, **290-293** (2001) 389.
[21] Wang W., Roth J., Lindig S. and Wu C. H., *J. Nucl. Mater.*, **299** (2001) 124.
[22] Andersen H. H., *Appl. Phys. A*, **18** (1979) 131.
[23] Frauenfelder R., *J. Vac. Sci. Technol.*, **6** (1969) 388.
[24] Ahlgren T., Heinola K., Vainonen-Ahlgren E., Likonen J. and Keinonen J., *Nucl. Instrum. Methods Phys. Res., Sect. B*, **249** (2006) 436.
[25] Vainonen-Ahlgren E., Ahlgren T., Likonen J., Lehto S., Sajavaara T., Rydman W. and Keinonen J., *Phys. Rev. B*, **63** (2001) 045406.
[26] Tsuchiya B. and Morita K., *J. Nucl. Mater.*, **220-222** (1995) 836.
[27] Sun G. Y., Friedrich M., Grötzschel R., Bürger W., Behrisch R. and Garćia-Rosales C., *J. Nucl. Mater.*, **246** (1997) 9.
[28] Franzen P., Behrisch R., Garćia-Rosales C., ASDEX Upgrade Team, Schleussner D., Rössler D., Becker J., Knapp W. and Edelmann C., *Nucl. Fusion*, **37** (1997) 1375.
[29] Masaki K., Sugiyama K., Tanabe T., Gotoh Y., Miyasaka K., Tobita K., Miyo Y., Kaminaga A., Kodama K., Arai T. and Miya N., *J. Nucl. Mater.*, **313-316** (2003) 514.
[30] Sugiyama K., Tanabe T., Krieger K., Neu R. and Bekris N., *J. Nucl. Mater.*, **337-339** (2005) 634.